JOURNAL OF AIRCRAFT
Vol. 48, No. 3, May–June 2011

Feedback-Controlled Forcefully Attached Flow on a Stalled Airfoil

Philipp Tewes* and Israel Wygnanski†
University of Arizona, Tucson, Arizona 85721
and
Anthony E. Washburn‡
NASA Langley Research Center, Hampton, Virginia 23681

DOI: 10.2514/1.C031168

Active maintenance of attached flow at natural poststall conditions requires a small intervention, relative to the one needed to force a separated flow to reattach under the same conditions. Experiments with slot suction applied near the leading edge of a stalled airfoil revealed a hysteresis of lift and drag that depends on the level of suction. This offers an opportunity to keep the flow attached at minimum input levels while guaranteeing that flow separation will not be allowed to occur. A simple approach was adopted that uses a rapidly responding pressure sensor located near the leading edge or in the interior reservoir of the airfoil for feedback control. The proposed controller used a prescribed pressure coefficient to keep the flow attached. Since a dimensionless pressure coefficient is required for this purpose, two similar sensors were installed in the pitot-static tube that monitored the freestream velocity. The impact of the time delay on the stability of the controller was briefly discussed and accounted for. The robustness of the controller was demonstrated under varying freestream velocities.

Nomenclature

C_d	=	drag coefficient
C_l	=	lift coefficient
C_p	=	pressure coefficient
$C_{p,1}$	=	C_p maximum threshold value
C_μ	=	steady momentum coefficient
$\langle C_\mu \rangle$	=	oscillatory momentum coefficient
c	=	chord length
ch	=	internal chamber
F^+	=	nondimensional frequency
h	=	slot width
i	=	iteration counter
LE	=	leading edge
p_s	=	supply pressure
Q	=	volume flow
Re	=	Reynolds number
TE	=	trailing edge
t	=	time
t_d	=	time delay
U	=	control voltage
U_m	=	voltage margin
$U_{\max}$	=	maximal voltage
U_s	=	stationary control voltage
U_∞	=	freestream velocity
x/c	=	nondimensional chord
x_{C_p}	=	center-of-pressure location
α	=	angle of attack
τ	=	pulse width
τ_D	=	dead time
τ_R	=	rise time
τ_V	=	vortex delay time

Presented as Paper 2008-4078 at the 4th Flow Control Conference, Seattle, WA, 23–26 June 2008; received 6 July 2010; revision received 30 November 2010; accepted for publication 12 December 2010.

*Research Associate, Department of Aerospace and Mechanical Engineering. Student Member AIAA.
†Professor, Department of Aerospace and Mechanical Engineering. Fellow AIAA.
‡Research Engineer, Flow Physics & Control Branch, Mail Stop 170. Senior Member AIAA.

I. Introduction

SEPARATED flow over a deflected flap, shown schematically in Fig. 1, could be forced to reattach by the introduction of periodic excitation (having no net mass flux) through the slot formed by the upper flap shoulder [1]. This was achieved for a wide spectrum of frequencies provided the amplitude of the perturbations was sufficiently large. It was observed that the most effective dimensionless frequencies requiring the smallest amplitude to force flow reattachment varied between $0.7 < F^+ < 1.5$. On the other hand, preventing attached flow from separating could be achieved at substantially lower amplitude, provided the frequency was also increased to a higher value of $F^+ > 2$. A very sensitive indicator in this case was that the center of pressure x_{C_p} fluctuated within the midflap region when the flow was separated, but moved closer to the leading edge for attached flow. An example of the movement of x_{C_p} with increased $\langle C_\mu \rangle$ at a predetermined frequency of $F^+ = 0.7$ is plotted in Fig. 2. At $\langle C_\mu \rangle = 25 \times 10^{-4}$ the flow reattached and x_{C_p} dropped from $\approx$0.5 to $\approx$0.2 (arrow 2). Thereafter, it was possible to reduce $\langle C_\mu \rangle$ by an order of magnitude (arrow 3) while keeping $x_{C_p} < 0.3$ before separation brought it back to the initial location. As long as the flow did not separate (arrow 3), one could increase or decrease the amplitude and the result was reversible. This seems to be a perfect opportunity for closed-loop control of separation, where one wants to fly under normal poststall conditions while keeping the flow attached. One wants to achieve this goal at minimum input of momentum and yet to ensure that separation will not be allowed to occur.

It was shown that the transient time of reseparation and reattachment of the flow on the generic flap [2,3] and on the GLAS II (Glauert Laminar Airfoil Section II) airfoil [4] scales with the time of flight between the actuator location and the trailing edge when periodic excitation is applied. This is associated with the amount of fluid that has to be entrained by the moving vortices created by the actuation and propagating downstream at a velocity that is proportional to the freestream velocity [2,3]. A basic understanding of the underlying physics is necessary for finding proper scaling of the transient time when constant suction or blowing replaces periodic

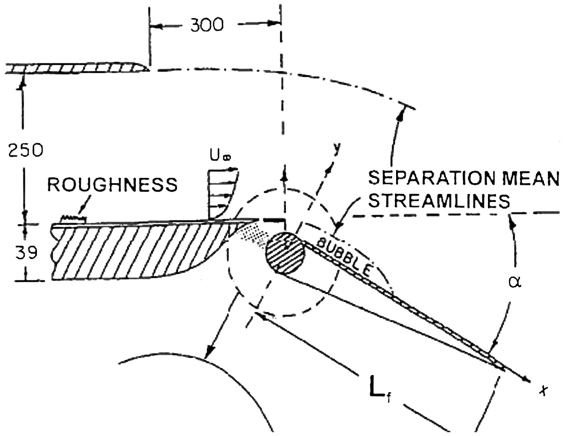

Fig. 1 Sketch of the generic flap [1].

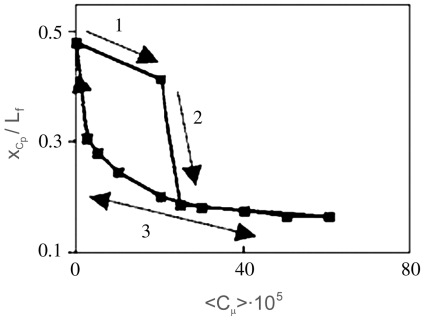

Fig. 2 Dependence of x_{C_p} [1] on $\langle C_\mu \rangle$ at $F^+ = 0.7$.

actuation. The knowledge of this scaling is most important for practical applications such as closed-loop control under varying flight speeds.

The closed-loop control strategy developed here is based on the identification of a hysteresis loop under predetermined flow conditions. Such a priori measurements consist of a series of open-loop tests, providing information about the threshold values of control authority, necessary for keeping the flow attached. Even for a single freestream velocity and angle of attack, the amount of work necessary to identify the process precisely, is significant; thus, for a series of freestream velocities and angles of attack emulating wind gusts, the identification part of the control strategy becomes daunting. The price of a control fault could be very high, since it may lead to an abrupt drop in lift and an increase in drag. This raises the need for a flexible control strategy, which will permit the control algorithm to safely adapt to the changing flow environment.

Very few experimental closed-loop separation control studies have been reported in the literature. Allan et al. [5] modeled the separated flow by a canonical second order system in order to improve the time response of the control strategy. Banaszuk et al. [6] used an extremum-seeking control algorithm to optimize the pressure recovery in a diffuser. More recently, Tian et al. [7] used nonlinear adaptive control of disturbance rejection to maximize the lift-to-drag ratio of the NACA 0025 airfoil. Pinier et al. [8] implemented the proportional control, based on proper orthogonal decomposition methodology, to flow separation. Becker et al. [9] used an extremum-seeking algorithm for the separation control. To the best of the authors' knowledge, no known attempts were made to take advantage of the earlier described hysteresis through a closed-loop control strategy. All of the above-mentioned closed-loop approaches achieved the control over a time scale that is much larger than that of the flow dynamics. The possible reason for that is the time delay between the control surge and the flow reaction, which could lower the anticipated performance of the control algorithms or, under certain conditions, even render them unstable.

The current approach is based on the simple closed-loop control of classical predictive logic, which applies known hysteresis measurements to the flow with fixed freestream conditions. The purpose of the present investigation is to validate and broaden the concept that uses hysteresis for closed-loop control through the application of constant suction. Suction was shown to be more effective [10] than blowing and as effective as zero mass net flux (ZMNF) in some instances for the elliptical airfoil used in this experiment.

II. Experimental Apparatus and Procedures

A. Model

The elliptical airfoil used in the present experiment has a chord of $c = 10.86$ in. (275.85 mm) and a maximum thickness of 30% chord. The circular cylinders that form its leading and trailing edges are 2.46 in. (62.48 mm) in diameter and they fit snugly into the main body of the airfoil. The slots are inclined at 30° to the local tangent and their width and location can be adjusted in situ by rotating the individual cylinders and placing the appropriate shim stock into the slots before tightening the end plates. For the current experiment the slot was fixed at 90° measured from the leading edge (LE) in a clockwise direction relative to the chord (see Fig. 3a). The slot pointed upstream and its width was $h = 0.015$ in. (0.38 mm). The symmetry of the configuration enables tests at positive and negative incidence angles by flipping the airfoil so that its trailing edge becomes a leading edge. One may also change the orientation of the slot relative to the oncoming stream. This might be very important near the leading edge, where acceleration of the flow away from the stagnation point (which is generally located on the lower surface) might affect the stall angle and the behavior of the airfoil near stall.

Data may be obtained by either placing the minor or the major axis of the ellipse normal to the flow. The major axis always represents the chord, and the minor one represents the maximum thickness of the elliptical airfoil. Under normal flight conditions, the major axis is inclined slightly to the oncoming stream. However, by rotating the

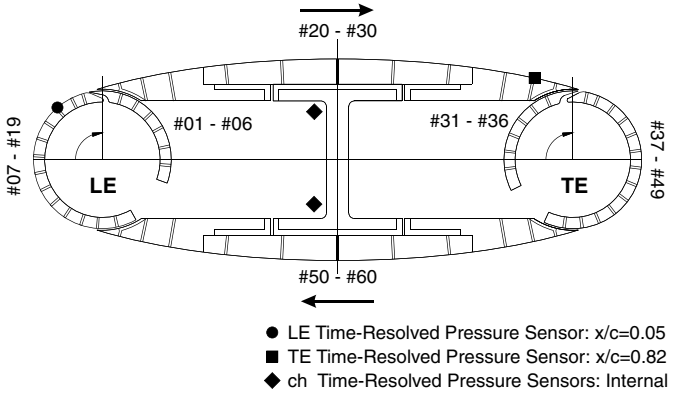

a) Tap and sensor distribution

b) Airfoil in test section

Fig. 3 Elliptical airfoil.

ellipse at 90° to the flow, the airfoil simulates the two-dimensional equivalent of a blunt body (e.g., helicopter fuselage or a tilt rotor wing in hover), thus measuring its download. An I-beam divides the interior volume of the airfoil into two independent pressure chambers through which steady blowing, suction, or a periodic ZMNF can be introduced either independently or in conjunction with one another.

The airfoil is equipped with 60 static-pressure taps (see Fig. 3), from which lift and form drag were calculated. Total drag was measured by traversing the wake three chord lengths downstream of the trailing edge, where the static-pressure corrections were small. The rake consists of 26 total-pressure probes that were placed at an interval of 1 in. (25.4 mm) and two static-pressure probes located at both ends of the rake. The wake rake could slide relative to the airfoil and could be centered in the wake. It could also be traversed across the wake in order to provide the necessary resolution of data points wherever the velocity gradients were steep. All the pressure ports were scanned electronically using a Pressure Systems, Inc., model 780 equipped with six 16-port differential pressure scanners. These scanners have an array of silicon piezoresistive pressure sensors, one for each pressure port. The sensors are calibrated by connecting them to a common manifold of known pressure.

The 24 in. (609.60 mm) span model was installed in a 36 by 24 in. (914.40 by 609.60 mm) test section of an open-loop, cascade wind tunnel. The Reynolds number tested varied between 150,000 and 500,000. To avoid the formation of laminar bubbles and the associated strong Reynolds number dependence, four roughness strips were used, two were placed at midchord ($x/c = 0.52$) and two at the juncture between the LE cylinder and the main element ($x/c = 0.12$). The installation of the airfoil in the tunnel is shown in Fig. 3b.

B. Open-Loop Control

For the open-loop control part of the experiment (Fig. 4a), the suction port of a single centrifugal blower was used for creating suction through the slot. This blower could provide up to 30 scfm (0.85 m^3/min) at a maximum pressure of 25 in H_2O (6227 Pa). The air leaving the settling chamber in the interior of the airfoil passed through two equal flexible hoses that were connected to each side of the settling chamber. The flow rate through the slot was regulated by changing the rpm of the blower and was monitored by using a specific flow meter.

C. Closed-Loop Control

For the closed-loop controlled experiment, two Venturi pumps (VACCON 750) were connected to both sides of the airfoil's interior chambers (plenums) to provide the required suction (see Fig. 4b). High-pressure air was supplied to these pumps through the proportionally controlled valve, which was regulated by a controller.

LabVIEW's [11] real-time (RT) module was used for the development and implementation of the closed-loop algorithm. The RT operational system (LabVIEW ETS) guarantees exact timing of the control process. The RT target used was a National Instruments (NI) PXI-1011, with a NI 8175 controller, equipped with an Intel Pentium III 866 MHz CPU. The host computer is a standard PC that runs LabVIEW RT and communicates with the RT target through the Ethernet. A NI PXI 6052E board fed the control signal to the valve controller. The control loop frequency was 1 kHz, and the worst-case time jitter was $\approx 60\ \mu s$.

Four dynamic pressure sensors, Endevco 85701C-1, were used as feedback signals to the controller. Two of the sensors were connected to the upper-surface taps of the airfoil: one upstream of the slot ($x/c = 0.05$) and the other close to the trailing edge ($x/c = 0.82$; see Fig. 3a). Two other sensors were connected to the pitot tube of the wind tunnel, permitting real-time normalization of the pressures converting them to C_p. Two more pressure sensors, Silicon Microstructure SM5652-015, were installed inside each chamber of the airfoil for monitoring the suction rate. All pressure sensors were connected through the SCXI 1520 unit to the target computer. The pressure signals were low-pass-filtered at 10 kHz.

D. Indirect Calibration Using Chamber Pressure

For proper characterization of the feedback performance, the correspondence between the applied control voltage and C_μ should be determined. Using the Venturi pumps in conjunction with the flow meter significantly degraded the pump's efficiency; thus, direct calibration of voltage vs C_μ was impossible. To overcome this difficulty, the calibration process was divided into two parts. In the first part, the volume flow passing through the suction slot was calibrated against the pressure in the interior chamber as seen in Fig. 5a. In the second part, the voltage supplied to the valve, feeding the Venturi pumps, was calibrated against the pressure in the same chamber (Fig. 5c), providing the necessary correlation between C_μ and the control voltage (Figs. 5b and 5d). A new calibration had to be performed for every freestream velocity and angle of attack providing different hysteresis loops for each flow condition.

III. Baseline Analysis

Baseline measurements were first carried out in order to document the flow characteristics of the airfoil. Differences in the airfoil characteristics (e.g., C_l and C_d) were found depending on whether the slot was sealed (Fig. 6) or open to the external flow (Fig. 7). The latter baseline was used for the purpose of comparison. Three freestream velocities (15, 20 and 25 m/s) were considered. The slope $dC_l/d\alpha$ was identical for all three freestream velocities considered and only slight differences were detected near stall. As seen, $C_{l,\max}$ is approximately 1.1 for the sealed slot (Fig. 6a) and was

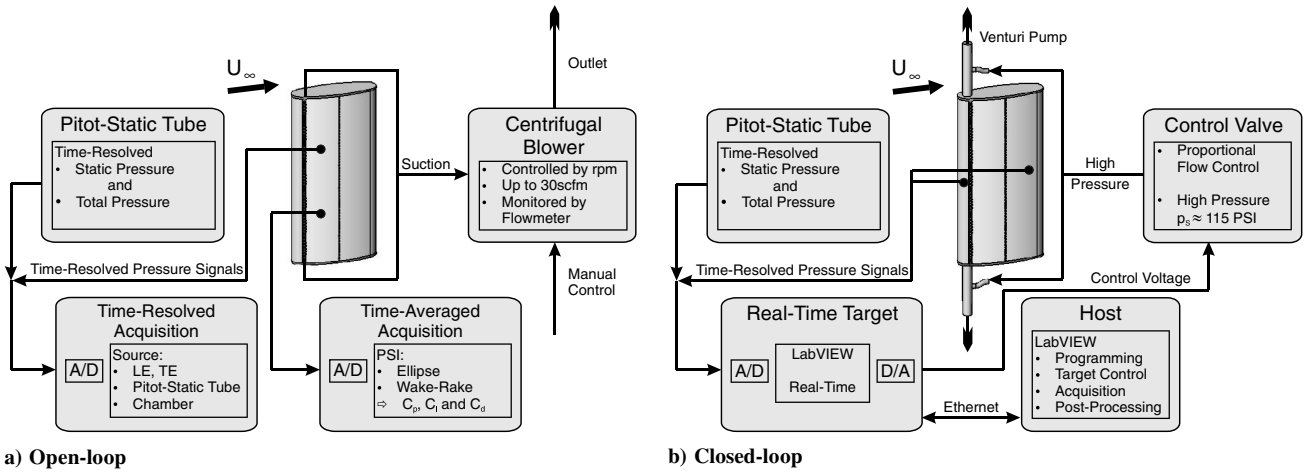

Fig. 4 Sketch of the experimental setup.

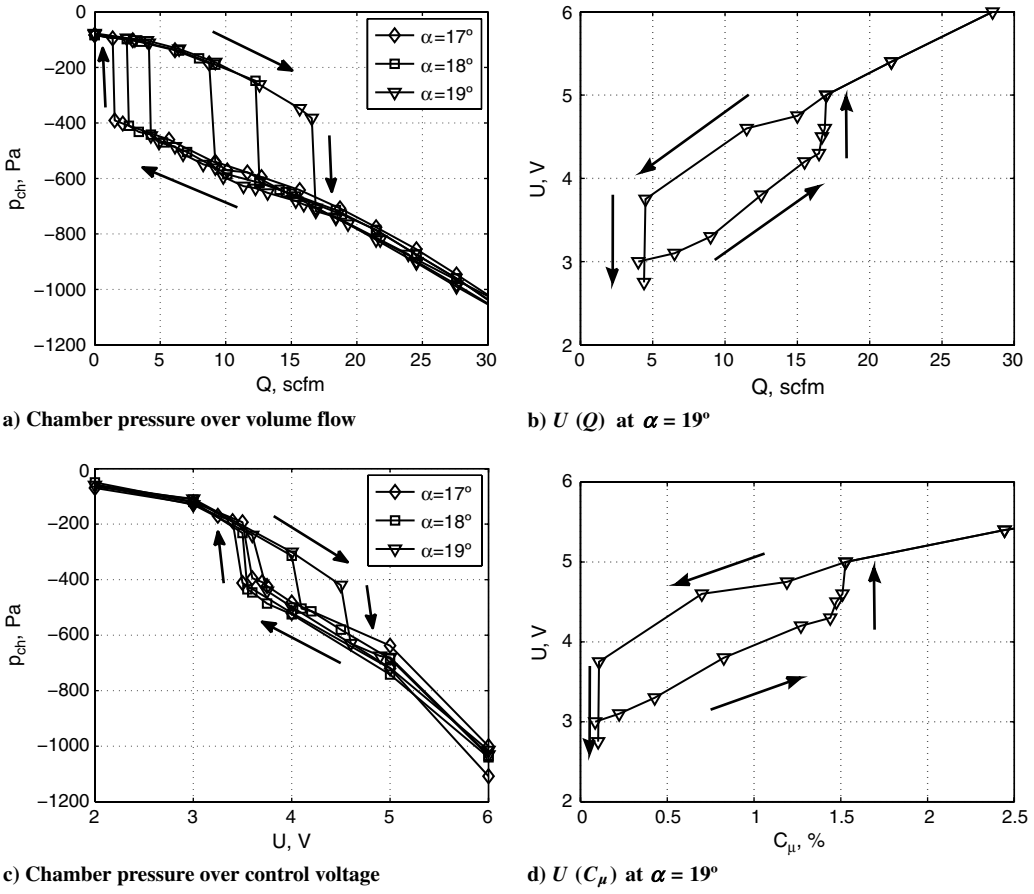

a) Chamber pressure over volume flow **b) U (Q) at $\alpha = 19°$**

c) Chamber pressure over control voltage **d) U (C_μ) at $\alpha = 19°$**

Fig. 5 Calibration results for $U_\infty = 15$ m/s.

assumed to be independent of the freestream velocity. The stall angle equals $\alpha = 16°$ for $U_\infty = 15$ m/s and it is seen to increase at higher velocities. The lift coefficient at poststall incidence is approximately 30% of $C_{l,\max}$. Decreasing α from its poststall values reveals that the flow reattaches at $\alpha = 15°$ for all freestream velocities considered. The observed hysteresis loop is typical for the thick airfoils.

The drag calculated by traversing the wake is shown in Figs. 6b and 7b. The drag coefficient is nearly constant ($\approx$0.09) as long as the flow is attached and increases to 0.35 after the occurrence of separation. The maximum values of lift and drag have decreased somewhat when the slot was open. The angles of separation and reattachment for $U_\infty = 20$ m/s and $U_\infty = 25$ m/s remained the same. However, for $U_\infty = 15$ m/s, both angles were reduced by 1°. These differences are attributed to Helmholtz resonances in the airfoil's cavity. Similar observations were made on the XV-15 airfoil [12].

Interestingly enough, a slight drop in C_l was observed when α was decreased just before flow reattachment. Pressure distributions along the airfoil (see Fig. 8a) revealed that a slightly adverse pressure gradient is generated on the upper surface, whereas the favorable $\mathrm{d}p/\mathrm{d}x$ was increased over most of the lower surface (i.e., for $0.15 < x/c < 0.70$). Furthermore, the pressure gradient decreased for higher x/c due to the upper surface. Close to the trailing edge, an adverse pressure gradient was observed (see Fig. 8b) to fulfill the Kutta condition. Both effects contribute to the observed reduction in C_l (Fig. 7a) before reattachment. Once the flow is reattached, $\alpha = 14°$, the suction peak around $x/c < 0.07$ is followed by an adverse pressure gradient along the upper surface. Separation occurs

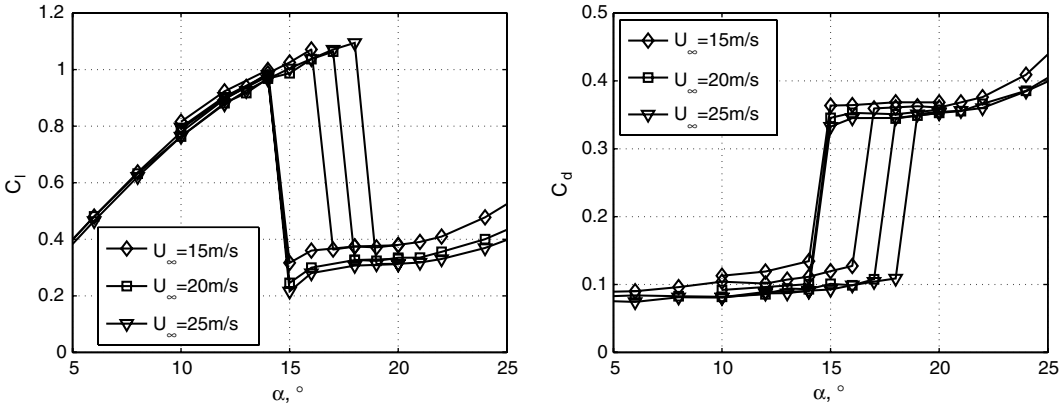

a) Lift **b) Drag**

Fig. 6 Baseline results for sealed slot.

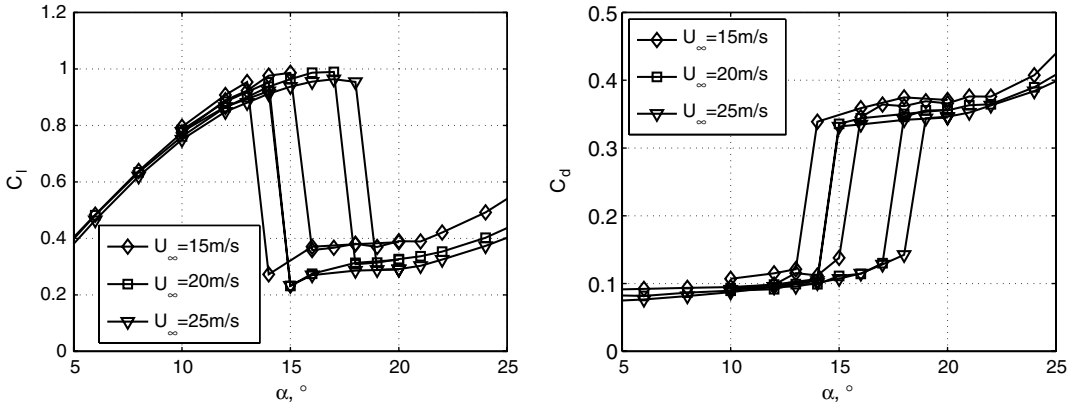

a) Lift **b) Drag**

Fig. 7 Baseline results for open slot.

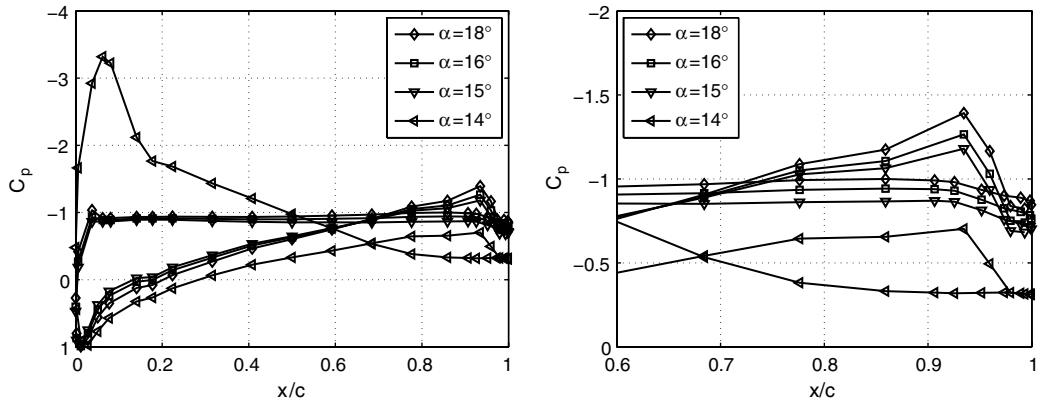

a) Pressure over airfoil **b) Pressure along trailing edge**

Fig. 8 Pressure distributions for decreasing α close to reattachment at $U_\infty = 20$ m/s.

only close to the trailing-edge region. This phenomenon could be observed for all freestream velocities considered.

IV. Open-Loop Control Results

The effect of suction on the airfoil at $Re = 2.5 \times 10^5$ is shown in Fig. 9. For the baseline case, separation progresses from the trailing edge upstream and that progression starts already at $\alpha = 8°$. Maximum lift, $C_{l,\max} = 1$, is obtained at $\alpha = 15°$ (Fig. 9a). Applying steady suction at $C_\mu = 1.7\%$ delays the stall angle by more than 10° and increases $C_{l,\max}$ to 2.1. The variations of C_d and C_l/C_d with α are plotted in Figs. 9b and 10a for a freestream velocity of $U_\infty = 15$ m/s. Because of the bluff trailing edge, the lift-to-drag ratio of this airfoil is less than 10 and suction increases it by a factor of 2.

Another indication of the difference between the attached- and separated-flow conditions is the wake. Wake surveys were made with and without suction applied to the airfoil. An example of two velocity profiles measured in the wake at $\alpha = 19°$ is plotted in Fig. 10b. The baseline curve corresponds to totally separated flow, whereas the other wake survey was carried out when the flow was attached due to the application of suction. Not only is the velocity deficit much larger

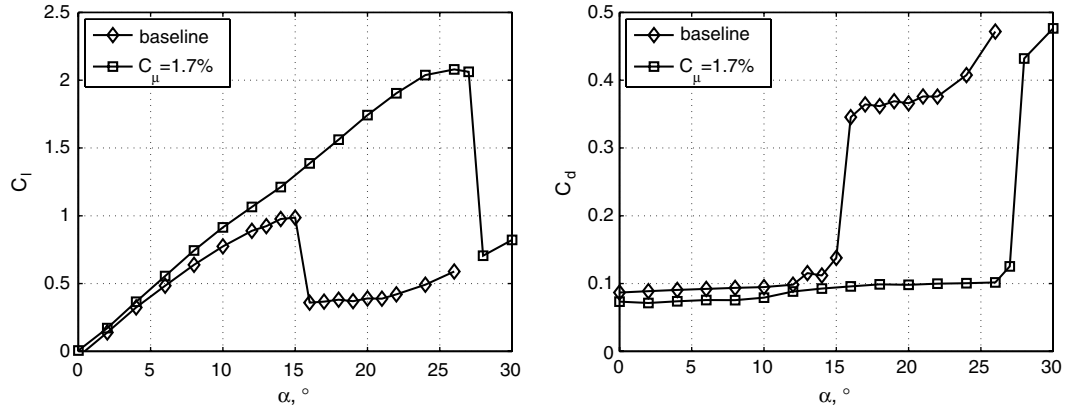

a) Lift **b) Drag**

Fig. 9 Lift and drag generated by the elliptical airfoil at $U_\infty = 15$ m/s.

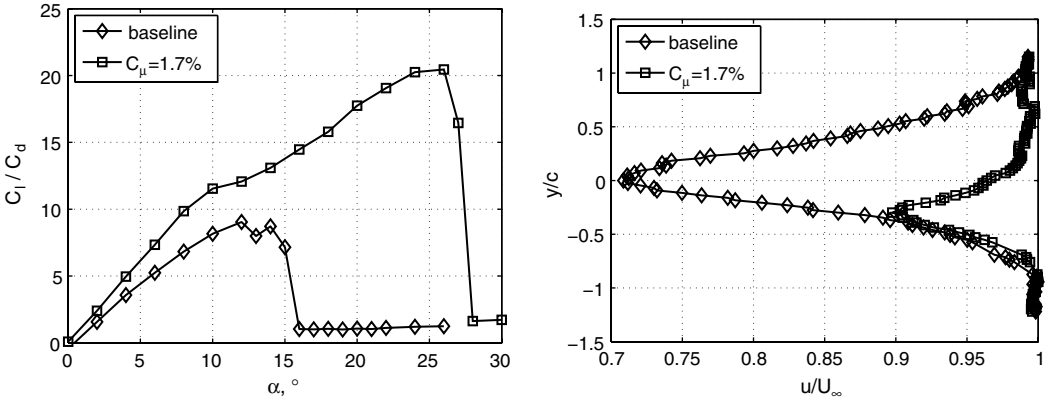

a) L/D **b) Velocity deficit at α = 19°**

Fig. 10 Lift-to-drag ratio and wake rake data at $U_\infty = 15$ m/s.

in the separated-flow case, but the mean location of the wake center differs by as much as 0.3 chord lengths. Closed-loop monitoring of the wake is impractical, however.

Details of the corresponding pressure distributions are shown in Fig. 11, where the differences between attached and separated flow are clearly seen due to the decrease in C_p at the trailing edge and significant reduction of C_p near the leading edge. The increase in C_l is an outcome of the elimination of the leading-edge bubble at $\alpha = 8°$ leading to total stall at $\alpha = 16°$, and the creation of the large suction peak in that region. This C_p decreased from its minimum value of $C_p = -2$ attained for the baseline (Fig. 11a), to a new minimum of $C_p = -7$, as shown in Fig. 11b for the controlled case.

The question that arises is how much suction is required to have the stalled airfoil recover at a prescribed incidence and freestream velocity. Starting with the baseline flow at $\alpha = 19°$ and increasing the suction incrementally, nothing much happens with the lift and drag coefficients until the suction momentum coefficient exceeds $C_\mu > 1.5\%$ as seen in Figs. 12a and 12b. When this threshold value is crossed, the flow reattaches to the upper surface, resulting in a decrease in drag (from $C_d = 0.36$ to $C_d = 0.11$) consistent with attached versus separated flow and a four-fold increase in lift. One may then reduce the suction level from the previous $C_\mu = 1.5\%$ to approximately 0.1% before a comparable reversal takes place. The implication is that it takes about 15 times larger C_μ to attach

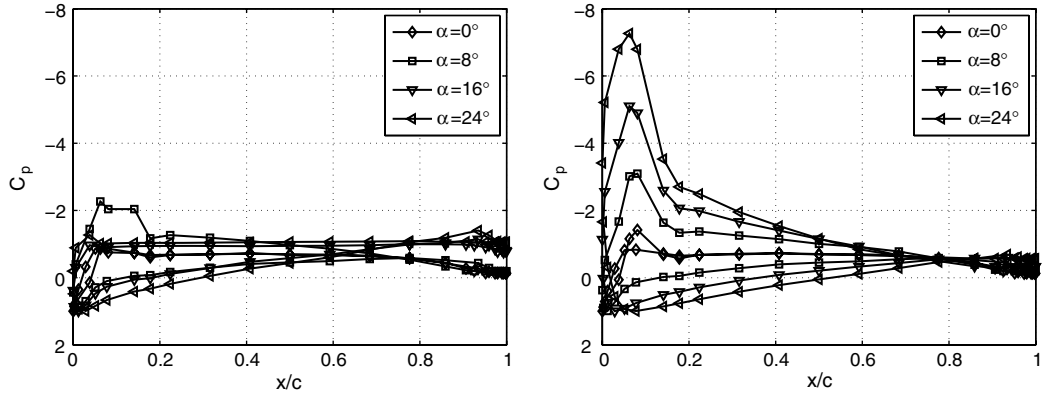

a) Baseline **b) Suction**

Fig. 11 Pressure distributions at $U_\infty = 15$ m/s.

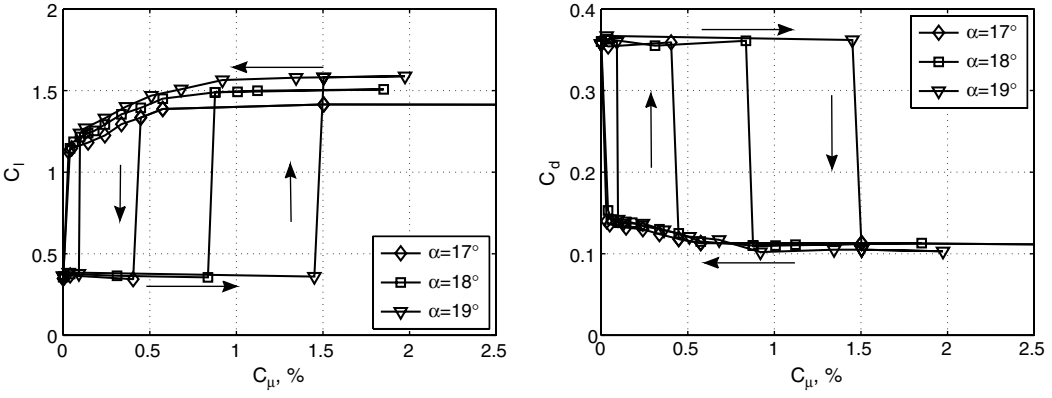

a) Lift **b) Drag**

Fig. 12 Hysteresis loops at $U_\infty = 15$ m/s.

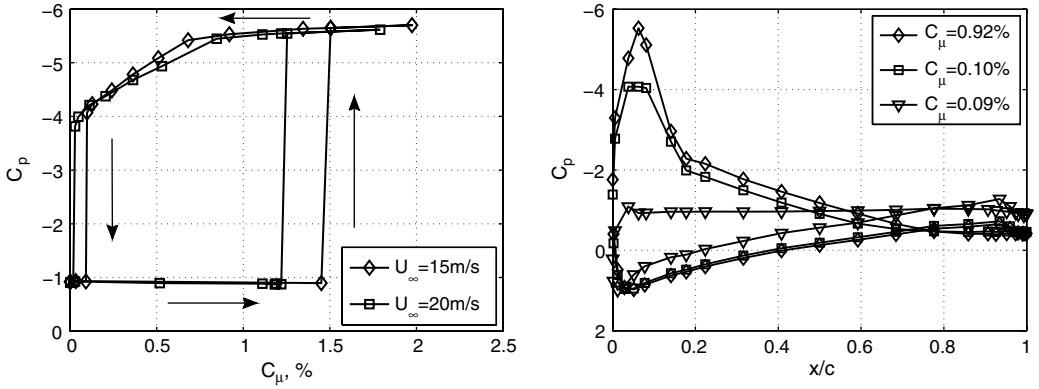

a) C_P at $x/c = 0.06$ **b) C_P over the airfoil at $U_\infty = 15\,m/s$, $\alpha = 19^o$**

Fig. 13 Pressure distributions at different levels of suction.

separated flow than to maintain attached flow under otherwise identical conditions. One hopes that by continuously monitoring the flow and controlling the suction parameters one could maintain attached-flow conditions at the lowest possible level of intervention and do so safely. This should be the purpose of proactive, closed-loop control of separation.

The hysteresis loop described in Fig. 12 can be reproduced at different angles of attack with different threshold values of C_μ. Tests at different freestream velocities indicate that flows at higher Reynolds numbers require a slightly lower threshold C_μ to reattach (Fig. 13a), and the threshold value at which separation occurs is also lower. This is due to the fact that at higher Reynolds numbers the boundary layer is thinner, thus requiring lower levels of suction to eliminate the momentum deficit generated by the boundary layer.

Pressure distributions on the upper surface of the airfoil (Fig. 13b) measured at $\alpha = 19°$ for various levels of C_μ (the flow was reattached before C_μ was reduced), suggest that C_p near the leading edge (i.e., $0.05 < x/c < 0.10$) is most sensitive to the state of the flow (Fig. 13b). The C_p drops from -5.5 to -1.0 when LE separation occurs. This fact is used in applying closed-loop control techniques to this flow. A sensor located at the leading edge was employed for deciding what control voltage, hence C_μ, should be applied to the controller. It should be remembered that C_p is much less sensitive to variations of the freestream velocity than the dimensional pressure; i.e., dimensionless criteria apply to all speeds and sizes. This fact is exploited in the closed-loop control part of the experiment, in which the admissible thresholds of C_p are specified, rather than the thresholds of the pressure.

A series of experiments, examining the dynamics of separation to be followed by reattachment were conducted by applying periodically controlled voltage pulses (unsteady suction) of different durations and amplitudes to the high-pressure valve that induces suction through the slot. The trailing-edge slot was sealed and hence was inactive. Depending on the relation between the pulse width τ and voltage the flow was either attached, separated, or partly attached, as could be deduced from the $C_{p,\mathrm{LE}}$ that were continuously monitored. It is clear that a fully open valve that uses a 10 V input for 600 ms, attaches the flow completely every time (see Fig. 14a). Reducing the amplitude and halving the duration (i.e., 7.5 V and 300 ms) fails to achieve complete reattachment for every event. One hundred repeated runs of each experiment were conducted to estimate the probability of reaching the prescribed C_p value, and the result is shown in Fig. 14b in terms of probability contours. Not surprisingly, the flow attaches for the time-voltage values, corresponding to the right upper corner.

The C_p outputs of three sensors (one in the interior of the airfoil's cavity, one located near the LE, and one near the trailing edge) were phase-locked to the input signal and are ensemble-averaged and plotted as a function of time in Fig. 15. The input signal was the one resulting in a complete reattachment of the flow (i.e., $U = 10$ V lasting for $\tau = 0.6$ s). Different freestream velocities were used in this experiment.

Different time scales are associated with the transient resulting with the initiation and termination of the suction. There is the dead time τ_D, i.e., the time delay required for the pressure to start dropping at the leading-edge sensor (Fig. 15c); the vortex-delay time τ_V, which corresponds to the time delay required for the trailing-edge sensor to record its first transient increase in pressure (Fig. 15e); and the rise time τ_R, which is represented by the steepest slope that would have reached a steady-state pressure (Fig. 15c).

The constant input voltage, applied at $\tau = 0$ ms, lowered the pressure in the interior chamber steadily (Fig. 15a). The time required to lower the pressure by a given increment was a constant, independent of the freestream velocity. The transient evacuation of the interior air by suction is likely to depend on the chamber volume, and it requires about 600 ms in the present case. On the other hand, the rise times and dead times sensed near the leading edge also depend on the freestream velocity, but this dependence is not simple,

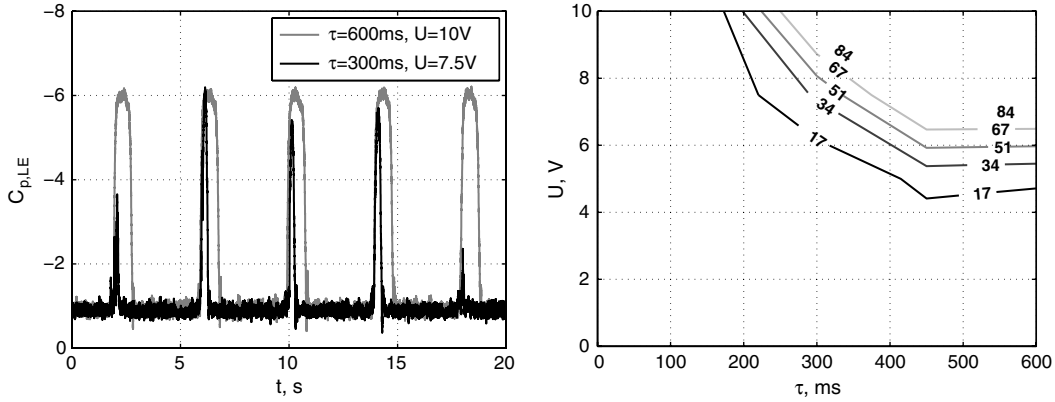

a) Time-resolved leading-edge sensor **b) Probability of reaching $C_p = -5.75$ in %**

Fig. 14 Statistical analysis for $\alpha = 19°$ at $U_\infty = 15$ m/s.

because the C_μ for a prescribed voltage input also depends on the freestream velocity. Once a threshold in the required coefficient is exceeded, the C_p near the leading edge starts to drop.

Since the pressure in the settling chamber did not reach a steady value during the 600 ms of suction application (Fig. 15a), additional tests of longer pulse duration were performed for comparison. For $\tau = 2000$ ms an equilibrium between the air volume (evacuated by the pump) and the volume (sucked through the slot) was achieved, resulting in a steady pressure in the chamber. No significant differences in the transient processes between the two cases of $\tau = 600$ and 2000 ms pulses were noticed in figures comparable to Figs. 15a–15f.

For the closed-loop applications, it is important to reduce the dead time observed near the leading edge of the airfoil, particularly when suction is used as a means for turbulence alleviations. This could be achieved by reducing the volume of the chamber.

The striking feature of the pressure signature at the trailing-edge sensor is the presence of substantial oscillations at the beginning of the reattachment and the separation processes (see Figs. 15e and 15f). Similar observations were made on the generic flap [2,3] and on the GLAS II [4] airfoil. In all those cases a dynamic stall vortex was created after the initiation of separation. In case of reattachment (see Fig. 15e), something akin to a "starting vortex" is accompanying the large increase in lift.

V. Closed-Loop Control Results

A. Simulation of the Delay Instability

The pressure on the upper surface of the airfoil does not respond instantly to a change in the actuation signal, as seen in Fig. 15c. Preliminary experiments were therefore carried out in order to assess the significance of this time delay on the controller's performance.

The flow, which was normally separated at $\alpha = 19°$ when the freestream velocity was $U_\infty = 15$ m/s, had always reattached whenever the control voltage applied to the suction pump was 8 V for a duration exceeding 400 ms. The voltage was then decreased in steps of 0.1 V/step at three different rates lasting 10, 50, and and 200 ms/step, as shown in Fig. 16. The pressure was continuously monitored by the LE and the interior chamber sensors, and the C_p coefficient was calculated at every step. When C_p sensed by the LE

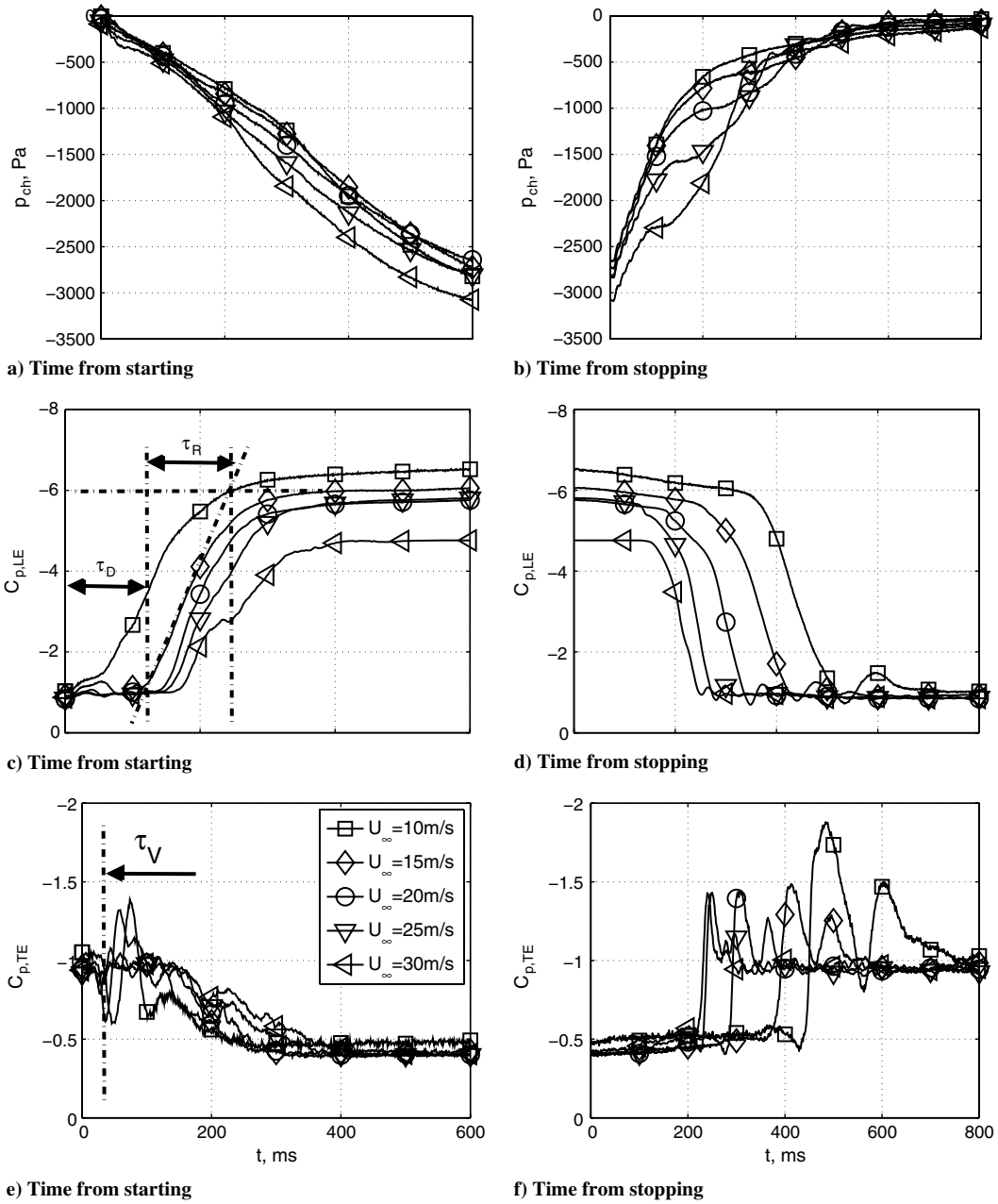

a) Time from starting

b) Time from stopping

c) Time from starting

d) Time from stopping

e) Time from starting

f) Time from stopping

Fig. 15 Time-resolved phase-averaged pressure signatures: $U = 10$ V, $\tau = 600$ ms at $\alpha = 19°$.

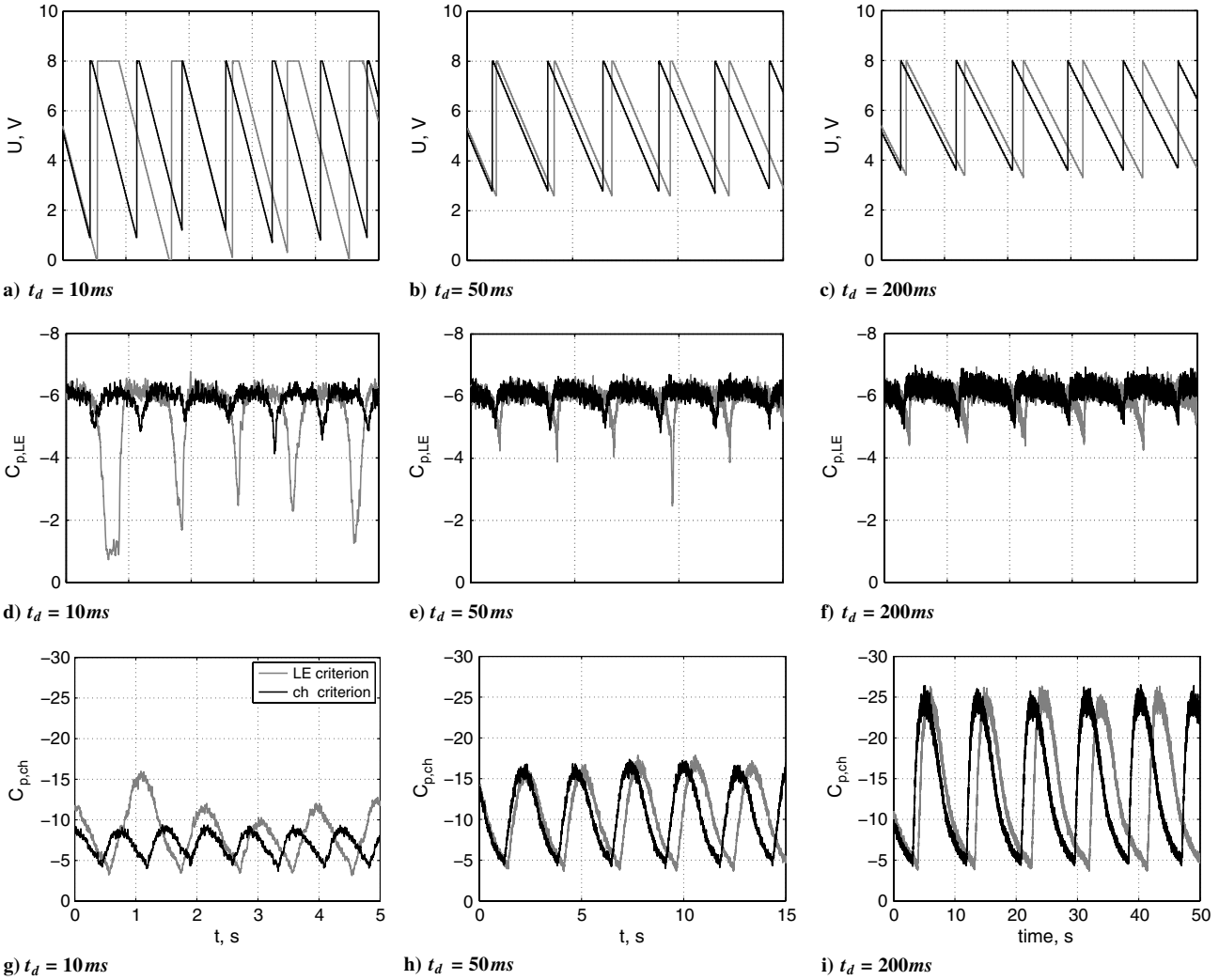

a) t_d = 10*ms* b) t_d= 50*ms* c) t_d = 200*ms*

d) t_d = 10*ms* e) t_d = 50*ms* f) t_d = 200*ms*

g) t_d = 10*ms* h) t_d = 50*ms* i) t_d = 200*ms*

Fig. 16 Time-delay observations on $C_{p,\mathrm{LE}}$ and $C_{p,\mathrm{ch}}$: $C_{p,\min} = -4.5$ at $U_\infty = 15$ m/s and $\alpha = 19°$.

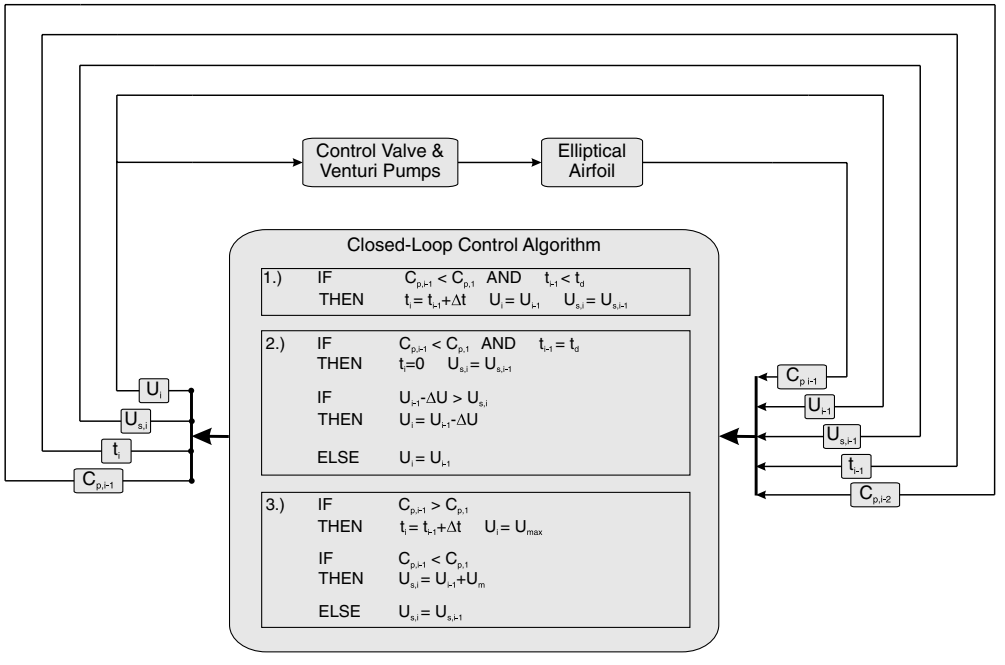

Fig. 17 Block diagram of the closed-loop control algorithm.

sensor exceeded the threshold value of −4.5, the controller immediately generated the maximum available voltage of 8 V, returning the flow to its attached state, and the entire process was repeated (Figs. 16a–16c). The increase in the LE C_p exceeded the prescribed value in all the cases considered; however, this excess depended on the rate at which the voltage was decreased. At the 10 ms/step, the measured LE C_p increased to approximately −2, and in one instance, the flow completely separated generating a LE $C_p \approx -1$ (Fig. 16d). In all three cases, the pressure read by the LE sensor (Figs. 16d–16f) lagged behind the control input implying that when a threshold C_p is sensed by the LE sensor, it is already too late to react, since the pressure in the interior of the chamber has risen above the pressure required for maintaining attached flow over the airfoil. The C_p measured in the interior of the airfoil did not lag behind the controller, but a minimum (maximum negative) value was proportional to the rate at which the controller's voltage was reduced. Thus, for the 10-ms-duration steps, the minimum values of $C_{p,\mathrm{ch}} \approx -10$ (Fig. 16g), and for the 2000 ms step it was $C_{p,\mathrm{ch}} \approx -25$ (Fig. 16i). The maximum value of the chamber pressure coefficient was clearly tied to the predetermined LE threshold value of −4.5, and it never exceeded $C_{p,\mathrm{ch}} \approx -5$ (Figs. 16g–16i). Thus, relying on the interior chamber pressure, rather than the LE C_p frees the controller from its previous dependence on the rate at which the voltage decreases.

Similar control performance was achieved when the chamber sensor was used for a feedback. This time, the interior pressure (Fig. 3a) was used as a criterion and the leading-edge sensor close to the surface was only monitored. The same set of experiments was repeated with the new criterion and plotted in Fig. 16. The measured voltage was similar to the voltage required by the leading-edge criterion. Analyzing the LE sensor response to the new criterion indicates that the flow near the LE never truly separated. There was no significant drop in C_p while varying the delay time. The pressure inside the chamber also seemed to be stable. No overshoots or distortion could be detected within the signal. Increasing the delay time forced the amplitude to rise to lower C_p values, since those values have the same order of magnitude as prescribed by the leading-edge criterion. A delay time of 200 ms was chosen for the current investigation, although this lengthy time per step will be reduced in the future.

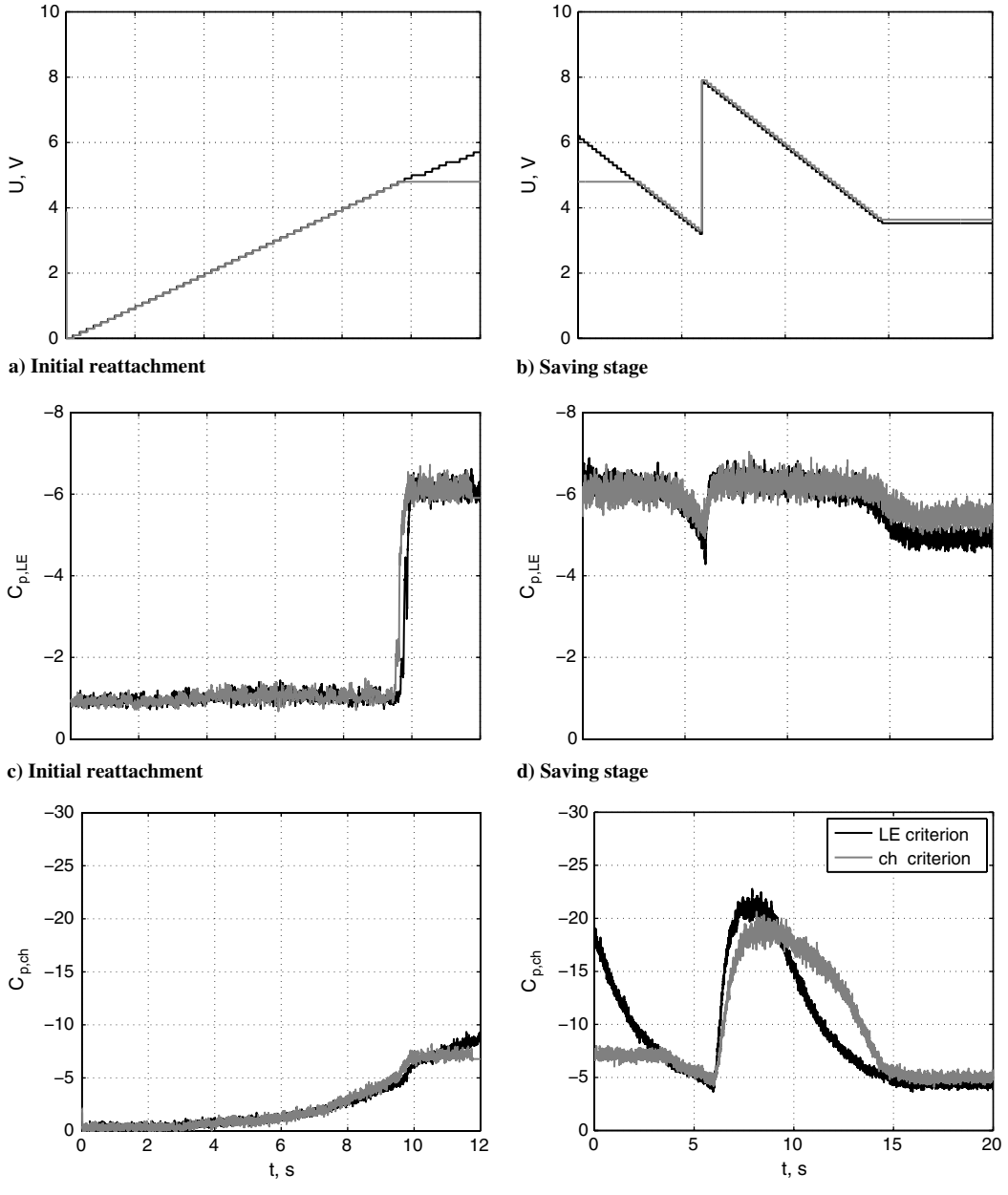

Fig. 18 Closed-loop control: criteria comparison for $U_\infty = 15$ m/s and $\alpha = 19°$.

B. Closed-Loop Algorithm

The purpose of the control algorithm is to keep the flow attached at the minimum input, which is tantamount to maintaining the C_p of the selected sensor below a prescribed threshold level $C_{p,1}$, determined in advance by an open-loop experiment. For example, the value of $C_{p,\mathrm{LE}} = -4.5$ could be taken as such a threshold for $U_\infty = 15$ m/s at $\alpha = 19°$ (Fig. 13). If the sensor detects that the threshold was reached, i.e., $C_p = C_{p,1}$, the control voltage is *instantaneously* increased to its maximum level, thus preventing flow separation. The control voltage, U_{i-1}, at which the threshold C_p was attained is used to define the new voltage level $U_{s,i}$ at which the flow would be attached, according to $U_{s,i} = U_{i-1} + U_m$, where U_m represents a safety margin. Then the voltage is slowly reduced to $U_{s,i}$ and if the flow conditions do not change, the flow is kept attached. Otherwise, the LE sensor detects the threshold and the control process recursively continues. The same procedure may be applied to the chamber sensor.

Let us now consider the operation of the closed-loop algorithm in more detail. The first stage is the identification of the minimal voltage that corresponds to the maximum permitted value of C_p defined by the user, based on the open-loop results. This is implemented by gradual stepwise decrease of the voltage until the threshold C_p value is achieved. For every voltage step the waiting interval is commensurate with the transient time, or else the premature low voltage level would cause separation. This is accomplished through instructions 1 and 2 given to the controller, shown schematically in Fig. 17. Accordingly the time counter t_i has to be larger than the time delay t_d if $C_{P,\mathrm{LE}}$ is used; thus, the voltage level will not be reduced, awaiting the reaction of the flow. If at some instance C_p becomes larger than the threshold $C_{p,1}$, the control voltage immediately increases to the prescribed maximum value $U_{\max}$ (instruction 3 given to the controller). $U_{\max}$ is chosen in advance to ensure that the flow will not separate. If $C_{p,i-1} > C_{p,1}$ occurs for the first time (i.e., $C_{p,i-2} < C_{p,1}$ then the corresponding voltage U_{i-1} is the critical voltage for the existing conditions, and the stationary voltage value is updated to $U_{s,i} = U_{i-1} + U_m$, where U_m provides a safety margin, taken as being 10% of U_{i-1}. If the occurrence of $C_{p,i-1} > C_{p,1}$ returns (i.e., $C_{p,i-2} < C_{p,1}$), the stationary voltage remains the same as in the previously sampled step. After several time steps the increase of voltage takes effect on the flow and $C_{p,i-1}$ becomes smaller than $C_{p,1}$. At this stage the controller follows instructions 1 and 2 and reduces the voltage slowly until the stationary voltage U_s is achieved. According to the previous identification stage this voltage is larger than the voltage, at which $C_{p,i-1} > C_{p,1}$ occurred, consequently, if the flow conditions do not change, the flow should remain attached at that control level. This closed-loop strategy provides substantial energy savings for a more efficient flow control.

C. Controller Demonstration

Before the initiation of the closed-loop control, the flow is forced to reattach by increasing C_μ corresponding to the lower branch of the $C_l(C_\mu)$ relationship shown in Fig. 12a. The time history of the applied voltage and the ensuing C_p coefficients are shown in Figs. 18a, 18c, and 18e. The voltage applied to the valve is increased by 0.1 V/step, unless the prescribed value of the $C_{p,\mathrm{LE}} = -2$ is attained. It was experimentally found that once this threshold $C_{p,\mathrm{LE}}$ value is exceeded, the flow would eventually reattach. Each applied voltage level lasted 200 ms to obviate the delay instability by accounting for the lag between the applied control and the flow reaction at the slot. Several sharp pressure pulses are the precursors of complete reattachments. To avoid errors when identifying the flow condition, the controller has to wait and determine if, after such oscillations, the pressure returns to its initial level requiring the voltage to increase until reattachment is complete. Changing the criterion to $C_{p,\mathrm{ch}} = -5$ could avoid this hesitancy.

An example of the savings achieved by using closed-loop control is shown in Figs. 18b, 18d, and 18f. Initially, the flow was attached by the process, described in Fig. 18a; however, the resulting control voltage needed to achieve this was high. At the beginning of the power-saving stage, the voltage was decreased by 0.1 V/step, until

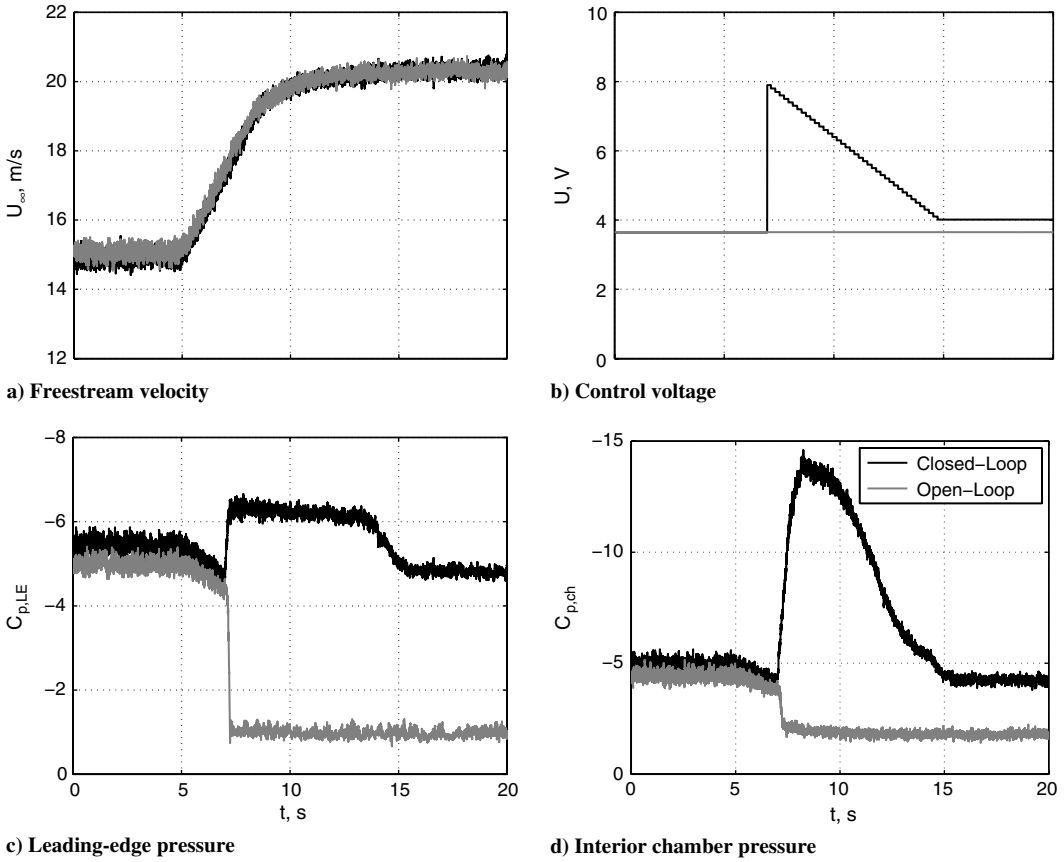

a) Freestream velocity **b) Control voltage**

c) Leading-edge pressure **d) Interior chamber pressure**

Fig. 19 Testing the robustness of the controller to changes in the freestream velocity at $\alpha = 19°$.

the separation threshold value $C_{p,1} = -4.5$ was achieved at the voltage $U_{i-1} \approx 3.1$ V. Then the control input was maximized to keep the flow attached and decreased again at the same rate to the voltage, which exceeded the value U_{i-1} by a 10% margin. This results in stably attached flow. The interior chamber pressure was also monitored, and its potential use as a feedback sensor was recognized. The power-saving stage enabled a voltage reduction of 1.5 V, corresponding to a reduction in C_μ ranging from 1.5 to 0.2% according to Fig. 5.

D. Robustness Analysis

To examine the robustness of the controller under consideration, the wind-tunnel speed was increased from $U_\infty = 15$ m/s to $U_\infty = 20$ m/s, thus reducing the C_μ of the suction that was maintained at a prescribed voltage level (Fig. 19). The wind-tunnel inertia resulted in a relatively long transient velocity time of approximately 5 s. The performances of the open-loop and the closed-loop controls were compared. Whereas the open-loop control failed to keep the flow attached by the constant 3.6 V supply, the closed loop performed well. Sensing impending separation, the controller increased the suction voltage to its original 8 V and then reduced it, stabilizing at 4 V to maintain $C_{p,\mathrm{LE}} < -4.5$. $C_{p,\mathrm{ch}}$ was also undergoing a transient that became stable at $C_{p,\mathrm{CH}} < -4.5$. In some cases, several control cycles (such as the one shown in Fig. 19b) are necessary for stabilization of the flow state.

Therefore, it seems that the chamber pressure parameter is more useful as an indicator for closed-loop control. The big advantage is that this parameter reacts faster than the leading-edge pressure parameter, thus making it possible to save more energy by quickly reducing U or C_μ. But the savings in energy is only for the dynamic part of the saving stage. The required energy for the steady stage after the saving stage was finished is higher than with the leading edge. This might void the described advantages. A combination of both criteria and the use of a weight function could combine the advantages of both criteria and lead to a powerful control tool in the future.

VI. Conclusions

The large difference between the level of suction required to force reattachment of separated flow and the level required to prevent separation from occurring under normally stalled conditions provides an opportunity for a closed-loop control strategy. The experiment carried out on the elliptical airfoil provides only one example of hysteresis that could occur on different configurations under different flow conditions that also use different flow control intervention techniques. Two additional flow control techniques (constant blowing and periodic excitation) were briefly tested, and they provided qualitatively similar results to those described above. Thus, the concept of the hysteresis feedback control was developed, permitting the flow to keep safely attached at the lowest possible input of energy.

It was found that when C_μ is reduced within the limits that keep the flow attached, the C_p measured near the leading edge was not significantly modified and the maximum C_p was not measured by an internal chamber sensor, enabling the use of either of those sensed values to be employed by the feedback controller. To eliminate the sensitivity to the freestream velocity variations, C_p has been used to define the feedback threshold level, rather than raw pressure readings. The impact of the time delay on the closed-loop control stability was discussed and demonstrated experimentally and some simple accounting of the delay was implemented in the controller. The robustness of the closed-loop control was demonstrated by varying wind-tunnel velocity, whereas the open loop failed to keep the flow attached, the closed loop succeeded to do so. The current investigation could be expanded to include the following developments:

1) C_l, and consequently C_p, values of the attached flow are significantly modified when the angle of attack changes concomitantly with a change in freestream velocity. For this reason, the current technique should be expanded to accept various threshold levels of $C_{p,\mathrm{ch}}$ and be amenable to changing flow angles of attack as well as speeds. A simple alternative could be based on a temporal derivative of C_p whose threshold exceeds a prescribed value. This might be used for turbulence alleviation that has to cope with simultaneous changes in both speed and incidence.

2) Predictive control, based on the system identification technique could be tried in this case, whereupon an a priori knowledge of flow dynamics becomes unnecessary.

3) Properties of the hysteresis should be carefully studied and documented, as they provide information about admissible control authority margins.

4) The detailed expansion of the current approach to other types of flow control, such as the use of zero-mass-flux actuation or sweeping jets, could result in significant benefits of lower required energy levels.

Acknowledgments

This research was supported by a NASA Research Announcement grant NNX07AB73A#1. The authors would also like to thank the work and effort put in by Boris Zakharin, whose input significantly contributed to the success of this project.

References

[1] Nishri, B. and Wygnanski, I., "Effects of Periodic Excitation on Turbulent Flow Separation from a Flap," *AIAA Journal*, Vol. 36, No. 4, 1998, pp. 547–556. doi:10.2514/2.428

[2] Darabi, A. and Wygnanski, I., "Active Management of Naturally Separated Flow over a Solid Surface. Part 1. The Forced Reattachment Process," *Journal of Fluid Mechanics*, Vol. 510, 2004, pp. 105–129. doi:10.1017/S0022112004009231

[3] Darabi, A. and Wygnanski, I., "Active Management of Naturally Separated Flow over a Solid Surface. Part 2. The Separation Process," *Journal of Fluid Mechanics*, Vol. 510, 2004, pp. 131–144. doi:10.1017/S0022112004009243

[4] Zakharin, B. and Wygnanski, I., "Forced Separation and Reattachment of Flow to Glauert Laminar Airfoil Section II," *Journal of Aircraft*, Vol. 45, No. 6, 2008, pp. 1991–2000. doi:10.2514/1.36027

[5] Allan, B., Juang, J. A. S, Pack, L., and Brown, D., "Closed-Loop Separation Control Using Oscillatory Flow," Inst. for Computer Applications in Science and Engineering, TR 2000-32, Hampton, VA, 2000.

[6] Banaszuk, A., Narayanan, S., and Zhang, Y., "Adaptive Control of Flow Separation in a Planar Diffuser," 41st Aerospace Sciences Meeting and Exhibit, Reno, NV, AIAA Paper 2003-0617, Jan. 2003.

[7] Tian, Y., Cattafesta, L., and Mittal, R., "Adaptive Control of Separated Flow," 44th AIAA Aerospace Sciences Meeting and Exhibit, Reno, NV, AIAA Paper 2006-1401, Jan. 2006.

[8] Pinier, J., Ausseur, J., Glauser, M. N., and Higuchi, H., "Proportional Closed-Loop Feedback Control of Flow Separation," *AIAA Journal*, Vol. 45, No. 1, 2007, pp. 181–190. doi:10.2514/1.23465

[9] Becker, R., King, R., Petz, R., and Nitsche, W., "Adaptive Closed-Loop Separation Control on a High-Lift Configuration Using Extremum Seeking," *AIAA Journal*, Vol. 45, No. 6, 2007, pp. 1382–1392. doi:10.2514/1.24941

[10] Chen, C., Zakharin, B., and Wygnanski, I., "On the Parameters Governing Fluidic Control of Separation and Circulation," 46th AIAA Aerospace Sciences Meeting and Exhibit, Reno, NV, AIAA Paper 2008-629, Jan. 2008.

[11] LabVIEW, Software Package, Ver. 8.5, National Instruments, Austin, TX, 2008.

[12] Stalker, A., Cerchie, D., Cullen, L., and Wygnanski, I., "Using Periodic Perturbations for Download Alleviation on Tilt-rotor Airplane Models in Hover," 2nd AIAA Flow Control Conference, Portland, OR, AIAA Paper 2004-2515, 2004.